COHESIVE SURFACE MODELING OF FAST CRACK GROWTH

A. NEEDLEMAN
Division of Engineering, Brown University
Providence, RI 02912 USA

ABSTRACT

A framework for modeling crack growth is described that is based on introducing one or more cohesive surfaces into a continuum. Constitutive relations are specified independently for the material and for the cohesive surfaces. Fracture emerges as a natural outcome of the deformation process, without introducing an additional failure criterion. The characterization of the mechanical response of a cohesive surface involves both an interfacial strength and the work of separation per unit area, which introduces a characteristic length into the formulation. Some results obtained from using this framework to analyze dynamic crack growth are discussed. The crack speed history and the mode of crack growth are outcomes of the analyses.

KEYWORDS

Dynamic fracture mechanics, computational modeling.

INTRODUCTION

In the traditional approach to fracture mechanics, the stress analysis is separated from a description of the actual process of material failure. A parameter characterizing the crack tip field, e.g. the energy release rate, is assumed to be a material property and known from experiment. Crack initiation is identified with this parameter reaching a critical value and the description of continued crack growth depends on knowing this parameter as a function of the amount of crack growth and the crack speed. Although this approach has been very successful, some observations seem to be difficult to account for within this framework; for example, the observation that limiting crack speeds in isotropic elastic solids are much less than the Rayleigh wave speed.

An alternative approach that will be discussed here is one where the failure characteristics are embodied in a phenomenological constitutive relation that describes separation along one or more cohesive surfaces, Needleman (1987). This differs from the classical cohesive zone models of Barenblatt (1962) and Dugdale (1960) in several respects; for example, an initial crack is not required to be present so that issues of nucleation of defects can be

addressed and the length of a cohesive zone is not a parameter of the model. This framework has been used to address a variety of issues; for example, void nucleation (Needleman, 1987; Tvergaard, 1990; Xu and Needleman, 1993); quasi-static crack growth (Tvergaard and Hutchinson, 1992); reinforcement cracking in metal-matrix composites (Finot *et al.*, 1994); interface fracture (Needleman, 1990; Tvergaard and Hutchinson, 1993; Xu and Needleman, 1995, 1996); and dynamic crack growth (Xu and Needleman, 1994; Siegmund and Needleman, 1996).

Within the cohesive surface framework in Needleman (1987), the continuum is characterized by constitutive relations that relate stress and deformation in the bulk material and that relate the traction and displacement jump across one or more cohesive surfaces. The parameters characterizing the cohesive surface separation law include a strength and the work of separation per unit area so that a characteristic length enters the formulation. These constitutive relations together with appropriate balance laws and initial and boundary conditions completely specify the initial/boundary problem. Fracture, when it occurs, emerges as a natural outcome of the loading history. No additional assumptions concerning crack initiation, crack propagation or crack branching criteria are needed.

The cohesive surface formulation and its finite element implementation are described for problems of crack growth under dynamic loading conditions. Some results obtained using this formulation are then discussed.

FORMULATION

The continuum is characterized by two constitutive relations. One is a volumetric constitutive law that relates stress and strain, while the other is a cohesive surface constitutive relation between the tractions and displacement jumps across a specified set of cohesive surfaces. Thus, there are two contributions to the internal virtual work; a volumetric contribution and a cohesive surface contribution. Using a Lagrangian description and finite strain kinematics, the principle of virtual work is written as

$$\int_V \mathbf{s} : \delta\mathbf{F} dV - \int_{S_{int}} \mathbf{T} \cdot \delta\mathbf{\Delta} dS = \int_{S_{ext}} \mathbf{T} \cdot \delta\mathbf{u} dS - \int_V \rho \frac{\partial^2 \mathbf{u}}{\partial t^2} \cdot \delta\mathbf{u} dV \tag{1}$$

In (1) the nominal stress tensor is denoted by $\mathbf{s}$, $\mathbf{u}$ is the displacement vector, $\mathbf{F}$ is the deformation gradient, $\mathbf{\Delta}$ is the displacement jump across a cohesive surface, $\mathbf{A} : \mathbf{B}$ denotes $A^{ij}B_{ji}$, V, S_{ext} and S_{int} are the volume, external surface area and internal cohesive surface area, respectively, of the body in the reference configuration. The density of the material in the reference configuration is ρ and the traction vector $\mathbf{T}$ and the reference configuration normal $\mathbf{n}$ are related by $\mathbf{T} = \mathbf{n} \cdot \mathbf{s}$. Also, $\mathbf{s} = \mathbf{F}^{-1} \cdot \boldsymbol{\tau}$, where $\boldsymbol{\tau}$ is the Kirchhoff stress, $\boldsymbol{\tau} = \det(\mathbf{F})\boldsymbol{\sigma}$, with $\boldsymbol{\sigma}$ being the Cauchy stress.

For an elastic cohesive surface constitutive relation,

$$\mathbf{T} = -\frac{\partial \phi}{\partial \mathbf{\Delta}} \tag{2}$$

An example of an elastic cohesive surface constitutive relation is one given in Xu and Needleman (1993). In two dimensions, with $\Delta_n = \mathbf{n} \cdot \mathbf{\Delta}$ and $\Delta_t = \mathbf{t} \cdot \mathbf{\Delta}$, where $\mathbf{n}$ denotes

the normal to the cohesive surface and $\mathbf{t}$ denotes the tangent to the cohesive surface, and with the direction of $\mathbf{n}$ specified so that positive Δ_n corresponds to increasing separation,

$$\phi(\Delta_n, \Delta_t) = \phi_n + \phi_n \exp(-\frac{\Delta_n}{\delta_n}) \left\{ \left[1 - r + \frac{\Delta_n}{\delta_n}\right] \frac{1-q}{r-1} - \left[q + (\frac{r-q}{r-1})\frac{\Delta_n}{\delta_n}\right] \exp(-\frac{\Delta_t^2}{\delta_t^2}) \right\} \tag{3}$$

with

$$q = \frac{\phi_t}{\phi_n} \qquad r = \frac{\Delta_n^*}{\delta_n} \tag{4}$$

where ϕ_n is the work of normal separation, ϕ_t is the work of tangential separation, δ_n and δ_t are normal and tangential cohesive characteristic lengths, respectively, and Δ_n^* is the value of Δ_n after complete shear separation under the condition of zero normal tension.

The work of separation, ϕ_n, is related to the tensile cohesive strength σ_{max} by

$$\phi_n = \sigma_{max} e \delta_n \tag{5}$$

where $e = \exp(1)$.

If the material is taken to be an elastic solid then $\mathbf{D} = \mathbf{D}^e$, where $\mathbf{D} = \text{sym}(\dot{\mathbf{F}} \cdot \mathbf{F}^{-1})$. Presuming small elastic strains and elastic isotropy,

$$\mathbf{D}^e = \mathcal{L}^{-1} : \hat{\boldsymbol{\tau}} \tag{6}$$

with $\hat{\boldsymbol{\tau}}$ the Jaumann rate of Kirchhoff stress and

$$\mathcal{L} = \frac{E}{1+\nu}\left[\mathbf{I}' + \frac{\nu}{1-2\nu}\mathbf{I} \otimes \mathbf{I}\right] \tag{7}$$

where E is Young's modulus, ν is Poisson's ratio, $\mathbf{I}$ and $\mathbf{I}'$ are the second and fourth order identity tensors, respectively, and $\otimes$ denotes the tensor product, $(\mathbf{A} \otimes \mathbf{B})^{ijkl} = A^{ij}B^{kl}$.

For a viscoplastic solid, the total rate of deformation, $\mathbf{D}$, is written as the sum of an elastic part, $\mathbf{D}^e$, and a viscoplastic part, $\mathbf{D}^p$, so that

$$\mathbf{D} = \mathbf{D}^e + \mathbf{D}^p \tag{8}$$

With the flow law taken to be that for a rate dependent Mises solid for which

$$\mathbf{D}^p = \frac{3\dot{\bar{\epsilon}}}{2\bar{\sigma}}\boldsymbol{\tau}' \tag{9}$$

where

$$\boldsymbol{\tau}' = \boldsymbol{\tau} - \frac{1}{3}(\boldsymbol{\tau} : \mathbf{I})\mathbf{I}\ , \quad \bar{\sigma}^2 = \frac{3}{2}\boldsymbol{\tau}' : \boldsymbol{\tau}' \tag{10}$$

$$\dot{\bar{\epsilon}} = R(\bar{\sigma}/g(\bar{\epsilon}))\ , \quad g(\bar{\epsilon}) = \sigma_0(\bar{\epsilon}/\epsilon_0 + 1)^N\ , \quad \epsilon_0 = \sigma_0/E \tag{11}$$

A superposed dot denotes differentiation with respect to time, $\bar{\epsilon} = \int \dot{\bar{\epsilon}} dt$, σ_0 is a reference flow strength, N is the strain hardening exponent and $R(\ )$ is a strain rate hardening function.

For pure power law rate hardening R is taken to be

$$R(x) = \dot{\epsilon}_1(x) = \dot{\epsilon}_0 x^{1/m} \tag{12}$$

where $\dot{\epsilon}_0$ is a reference strain rate and m is the strain rate hardening exponent.

In order to model enhanced strain rate sensitivity at high strain rates, R can be specified as

$$R(x) = \frac{\dot{\epsilon}_1(x)\dot{\epsilon}_2(x)}{\dot{\epsilon}_1(x) + \dot{\epsilon}_2(x)} \tag{13}$$

with $\dot{\epsilon}_1(x)$ given by (12) and

$$\dot{\epsilon}_2(x) = \dot{\epsilon}_m \exp\left[-\frac{a}{x}\right] \tag{14}$$

where $\dot{\epsilon}_m$ and a are strain rate hardening parameters.

The finite element method is used to discretize (1). The only difference from the formulation for a conventional continuum problem comes from the cohesive contribution to the internal virtual work, the surface integral on the left hand side of (1). The analyses discussed here are two dimensional and quadrilateral elements are used, each of which is built up from four "crossed" linear displacement triangular elements. When the discretized representation of the displacement field is substituted into the principle of virtual work (1) and the integrations are carried out, the discretized equations of motion are obtained as

$$\mathbf{M}\frac{\partial^2 \mathbf{U}}{\partial t^2} = \mathbf{R} \tag{15}$$

where $\mathbf{U}$ is the vector of nodal displacements, $\mathbf{M}$ is the mass matrix and $\mathbf{R}$ is the nodal force vector consisting of contributions from the area elements and the cohesive surfaces.

A lumped mass matrix is used together with an explicit time integration scheme to obtain the nodal velocities and the nodal displacements. Once the displacements and velocities at the end of the time step are known the deformation gradient, the strain rate, the displacement jump across a cohesive surface and other kinematic quantities can be directly calculated. The volumetric and cohesive surface constitutive relations are then used to obtain updated values of the remaining field quantities of interest. For an elastic cohesive surface constitutive relation, the tractions across the cohesive surface can be calculated directly from the displacement jump. The material constitutive relations are then integrated so that all quantities are known that are needed to compute the response for the next time step.

RESULTS

The cohesive surface framework has been used to address a variety of issues in dynamic crack growth. A few illustrative results are presented in the following. In all cases, the specimen analyzed is a center cracked plate subject to tensile impact loading. Plane strain conditions are presumed. In some cases, the crack is constrained to grow straight ahead, while in other cases the crack path is an outcome of the analysis. Complete specification of the analysis parameters, along with additional results, are given in the references cited.

Crack Branching in Homogeneous Elastic Solids

In Xu and Needleman (1994) calculations with a crude 40×40 quadrilateral mesh were used to analyze qualitative features of dynamic crack growth behavior in elastic solids.

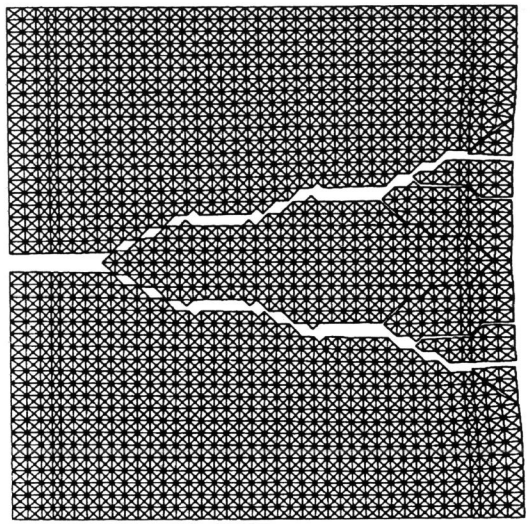

Figure 1: Deformed finite element mesh illustrating the predicted mode of crack branching.

Figure 1 shows the crack branching pattern (only the right half of the specimen is shown). Although the mesh is not fine enough to resolve detailed fields around the crack tip, the result illustrates characteristic features of observed modes of brittle fracture. For example, although crack branching was restricted to being perpendicular to the current crack line or along $\pm 45°$ diagonals, the overall branching angle was $\approx 30°$ from the initial crack line. This crack branching angle is in good agreement with what was found for a much finer mesh. It was also found in Xu and Needleman (1994) that the amount of straight crack growth prior to branching decreased with increasing impact velocity.

Figure 2, from Xu and Needleman (1994), shows a curve of crack speed versus time for a fine mesh calculation (the mesh has 336,000 triangular elements and 2,016,000 degrees of freedom). For comparison purposes, the crack speed versus time curve for the same block size and loading conditions is shown where the crack is constrained to grow straight ahead. The crack speed at first increases smoothly, then an oscillating crack speed versus time curve is obtained. The crack speed reaches about 420 m/s ($0.45c_R$) before the first large oscillation in crack speed, which occurs between $t = 1.40$ μs and $t = 1.42$ μs. This is shortly before the arrival of a reflected stress wave at $t = 1.44$ μs. There are then some high frequency, relatively low amplitude oscillations in crack speed followed by an attempted branching that gives rise to the large drop in crack speed at $t = 1.57$ μs. Crack growth then resumes on the initial crack plane and the crack speed increases. The crack bifurcates into two branches at about $t = 1.75$ μs. In the latter stages of crack growth the mean crack speed is ≈ 350 m/s ($\approx 0.37c_R$). The oscillations in crack speed for the calculation with unconstrained crack growth are of larger amplitude and lower frequency than the discretization induced fluctuations. Such oscillations in crack speed versus time

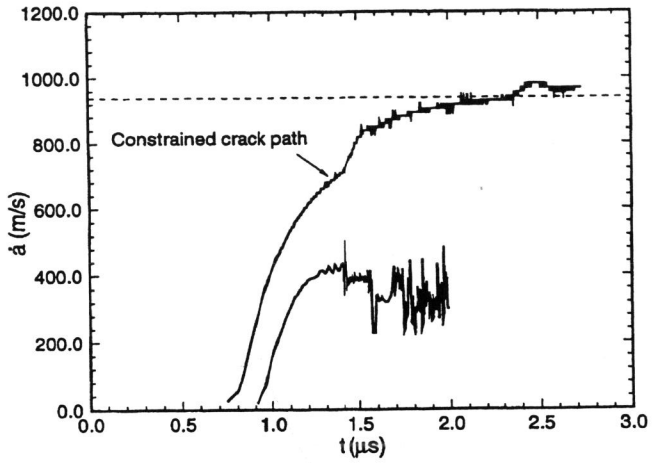

Figure 2: Crack speed, $\dot{a}$, versus time, t. For comparison purposes, the crack speed versus time curve with crack growth constrained to occur along the initial crack plane is also shown. The dashed line shows the Rayleigh wave speed.

have been observed by Fineberg *et al.* (1992). Crack branching is what limits the crack speed for an elastic solid to less than half the Rayleigh wave speed in the analysis of Xu and Needleman (1994).

Dynamic Crack Growth Along an Interface

Results from Xu and Needleman (1996) for a PMMA/Al bimaterial with impact loading on the PMMA side are shown in Fig. 3. The crack is constrained to grow along the bond line. Figure 3a shows curves of crack speed, $\dot{a}$, versus time. Crack growth starts soon after the arrival of the loading wave at $t = 1.34\mu$s. Because of the impedance mismatch across the bond line, some of the wave is reflected and some is transmitted. The transmitted wave is reflected back by the fixed boundary at the opposite edge and arrives at the interface at $t = 2.23\mu$s which causes an increase in crack speed. The crack speed exceeds the Rayleigh wave speed of PMMA and then decreases a little when the compressive reflected wave arrives at $t = 3.11\mu$s. For comparison purposes, crack speed versus time curves for a homogeneous PMMA specimen, with the same bond line cohesive properties, are shown in Fig. 3a for impact velocities, V_1, of 30 m/s and 15 m/s. Since both halves of the specimen are PMMA, there are no wave reflections along the bond line. Crack growth starts soon after the arrival of the loading wave at $t = 1.34\mu$s and the crack speed rapidly reaches a constant. With an impact velocity of 30 m/s, this constant is the Rayleigh wave speed while with an impact velocity of 15 m/s, the limiting crack speed is 89 % of the Rayleigh wave speed. For a given impact velocity, the interface crack reaches a higher speed than does a corresponding crack in a homogeneous solid. Also, the crack acceleration, the time interval over which the more or less steady crack speed is reached, is smaller for the interface crack

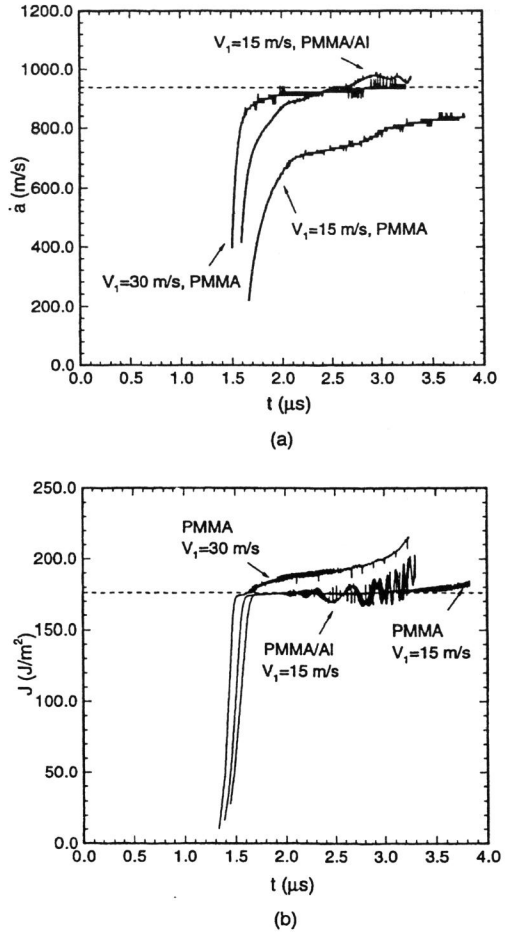

Figure 3: Crack speed, $\dot{a}$, versus time, t, (a) and J-integral versus time (b) for an interface crack between PMMA and aluminum. For comparison purposes results are also shown for homogeneous PMMA. In (a) the dashed line indicates the Rayleigh wave speed of PMMA and in (b) the dashed line corresponds to the work of separation.

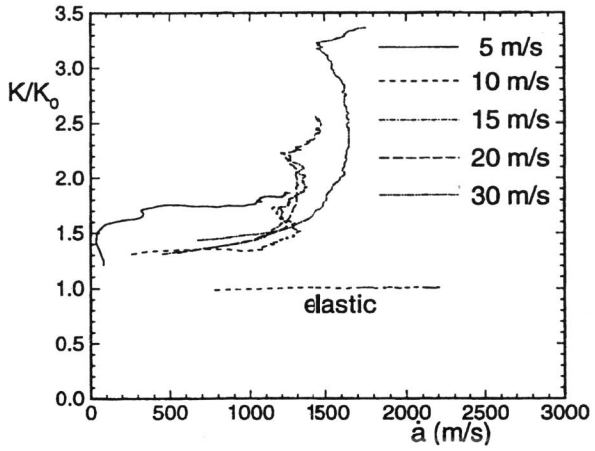

Figure 4: Normalized stress intensity factor, K/K_0, versus crack speed, $\dot{a}$, for power law strain rate hardening and with various values of impact velocity. For comparison purposes, results from a calculation with elastic material behavior are also shown.

than for the homogeneous solid.

Curves of the J-integral versus time are shown in Fig. 3b for the three cases in Fig. 3a. Crack growth begins when J has increased to ϕ_n, as it should, Rice (1968). For homogeneous PMMA, J is nearly constant during the early stages of crack growth; with $V_1 = 15$ m/s, J slowly exceeds ϕ_n, while with $V_1 = 30$ m/s, J increases more rapidly. For the crack along the PMMA/Al bimaterial interface, growth also initiates when $J \approx \phi_n$, J is then nearly constant for some time interval and then oscillates. The mean value of J increases as the crack speed increases.

Since the crack is subject to tensile loading, the mode of crack growth in homogeneous PMMA is mode I. On the other hand, for the PMMA/Al interface crack, the mode of crack opening involves both mode I and mode II components, with an increasing mode II contribution as the crack speed increases.

Dynamic Crack Growth in a Viscoplastic Solid

Siegmund and Needleman (1996) analyzed the effect of viscoplastic material response on dynamic crack growth with the crack constrained to grow straight ahead. Computed curves of normalized stress intensity factor, K/K_0, versus crack speed, $\dot{a}$, are shown in Fig. 4 where K is defined in terms of the computed value of J using the small scale yielding relation $K = \sqrt{EJ/(1-\nu^2)}$. There is a strong upturn in the stress intensity factor as the crack speed increases. For a viscoplastic solid, the combination of material inertia and dissipation act to limit the attainable crack speed even when the crack is constrained to

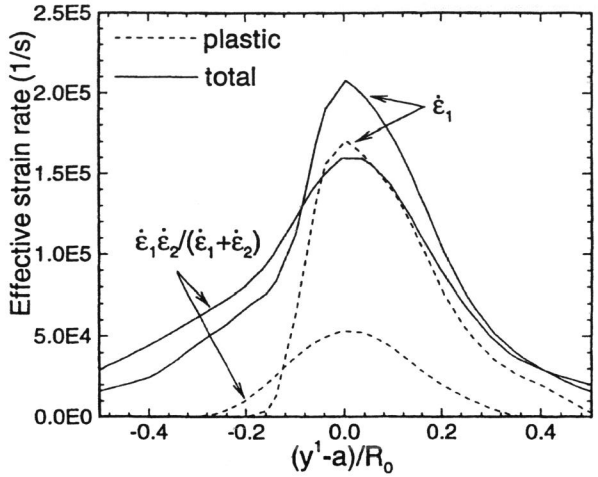

Figure 5: Distribution of equivalent plastic and equivalent total strain rate at the crack tip; values are taken 0.06 mm above the crack in the deformed configuration.

grow along the initial crack line. By way of contrast, in Xu and Needleman (1994) for an elastic solid, crack branching limits the crack speed.

The dependence of stress intensity factor on crack speed in Fig. 4 is consistent with experimental observations, see e.g. Rosakis and Zehnder (1985) and Zehnder and Rosakis (1990). While there clearly is not a one-to-one correspondence between the value of the stress intensity factor and the crack speed, three cases, those with impact velocities of 10 m/s, 15 m/s and 20 m/s, fall within a fairly narrow band. For these cases, the crack speed at which the sharp increase in K takes place, ≈ 1200 m/s (the Rayleigh wave speed is 2987 m/s), is in good agreement with the experimental values in Rosakis and Zehnder (1985) and Zehnder and Rosakis (1990). Lam and Freund (1985) and Freund (1990) found the stress intensity factor to be a strongly increasing function of crack speed in computations where dynamic crack growth in a plastic solid was assumed to occur at a constant speed. In the cohesive surface formulation, the crack speed history, as well as the history of K, are outcomes of the analysis.

The near-tip strain rates for the power law strain rate hardening and enhanced strain rate hardening materials are compared in Fig. 5. This figure shows curves of effective plastic strain rate, $\dot{\bar{\epsilon}}$ and total effective strain rate, $\dot{\epsilon}_{eff}$, versus distance from the current crack tip. The total effective strain rate is defined by

$$\dot{\epsilon}_{eff} = \sqrt{\frac{2}{3}\mathbf{D}:\mathbf{D}} \tag{16}$$

For the power law strain rate hardening material, the curves labeled $\dot{\epsilon}_1$, the main contribution to the peak total strain rate is the plastic strain rate. On the other hand, for the

material with enhanced strain rate hardening, labeled $\dot{\epsilon}_1\dot{\epsilon}_2/(\dot{\epsilon}_1 + \dot{\epsilon}_2)$, the peak strain rate is mainly elastic. The enhanced strain rate hardening at high strain rates was found to lead to less plastic straining and a more brittle response. The stress distributions with enhanced strain rate hardening were also found to become more like those for an elastic growing crack than for the power law rate hardening material.

The dominance of elastic strain rates and a change in the character of the crack tip fields to the elastic fields are key assumptions of the analysis of dynamic crack growth in Freund and Hutchinson (1985). The analyses in Siegmund and Needleman (1996) suggest that these are reasonable approximations in the enhanced strain rate hardening regime.

CONCLUDING REMARKS

The cohesive surface formulation and its finite element implementation for dynamic loading problems have been described and calculations for elastic and viscoplastic solids have been discussed. Once the constitutive relations for the material and the cohesive surface are prescribed, fracture is an outcome of the initial/boundary value problem solution. No additional crack initiation, crack growth or crack branching criteria are specified. The formulation contains a characteristic length so that convergent predictions for fracture can be obtained. This formulation also lends itself to analyzing crack growth along more or less arbitrary paths, as in Xu and Needleman (1994, 1995).

ACKNOWLEDGEMENTS

Support from the Air Force Office of Scientific Research under grant F49620-94-1-0300 and from the Office of Naval Research under grant N00014-89-J-3054 is gratefully acknowledged.

REFERENCES

Barenblatt, G.I. (1962) Mathematical theory of equilibrium cracks. *Adv. Appl. Mech.* **7**, 56-129.

Dugdale, D.S. (1960) Yielding of steel sheets containing slits. *J. Mech. Phys. Solids* **8**, 100-104.

Fineberg, J., Gross, S.P., Marder, M. and Swinney, H.L. (1992) Instability in the propagation of fast cracks. *Phys. Rev.* **B45**, 5146-5154.

Finot, M., Shen, Y.-L., Needleman, A. and Suresh, S. (1994) Micromechanical modelling of reinforcement fracture in particle-reinforced metal-matrix composites. *Metall. Mater. Trans.* **25A**, 2403-2420.

Freund, L.B. (1990) *Dynamic Fracture Mechanics*. Cambridge University Press, Cambridge.

Freund, L.B. and Hutchinson, J.W. (1985) High strain-rate crack growth in rate-dependent plastic solids. *J. Mech. Phys. Solids* **33**, 169-191.

Lam, P.S. and Freund, L.B. (1985) Analyses of dynamic growth of a tensile crack in an elastic-plastic material. *J. Mech. Phys. Solids* **33**, 153-167.

Needleman, A. (1987) A continuum model for void nucleation by inclusion debonding. *J. Appl. Mech.* **54**, 525-531.

Needleman, A. (1990) An analysis of tensile decohesion along an interface. *J. Mech. Phys. Solids* **38**, 289-324.

Rice, J.R. (1968) A path independent integral and the approximate analysis of strain concentration by notches and cracks. *J. Appl. Mech.* **35**, 379-386.

Rosakis, A.J. and Zehnder, A.T. (1985) On the dynamic fracture of structural metals. *Int. J. Frac* **27**, 169-186.

Siegmund, T. and Needleman, A. (1996) A numerical study of dynamic crack growth in elastic-viscoplastic solids. *Int. J. Solids Struct.*, to be published.

Tvergaard, V. (1990) Effect of fibre debonding in a whisker-reinforced metal. *Mater. Sci. Eng.* **A125**, 203-213.

Tvergaard, V. and Hutchinson, J.W. (1992) The relation between crack growth resistance and fracture process parameters in elastic-plastic solids. *J. Mech. Phys. Solids* **40**, 1377-1392.

Tvergaard, V. and Hutchinson, J.W. (1993) The influence of plasticity on mixed mode interface toughness. *J. Mech. Phys. Solids* **41**, 1119-1135.

Xu, X.-P. and Needleman, A. (1993) Void nucleation by inclusion debonding in a crystal matrix. *Modell. Simul. Mater. Sci. Eng.* **1**, 111-132.

Xu, X.-P. and Needleman, A. (1994) Numerical simulations of fast crack growth in brittle solids. *J. Mech. Phys. Solids* **42**, 1397-1434.

Xu, X.-P. and Needleman, A. (1995) Numerical simulations of dynamic interfacial crack growth allowing for crack growth away from the bond line. *Int. J. Fract.* **74**, 253-275.

Xu, X.-P. and Needleman, A. (1996) Numerical simulations of dynamic crack growth along an interface. *Int. J. Fract.* **74**, 289-324.

Zehnder, A.T. and Rosakis, A.J. (1990) Dynamic fracture initiation and propagation in 4340 steel under impact loading. *Int. J. Frac* **43**, 271-285.